Line-defects-mediated complex-oscillatory spiral waves in a chemical system

Jin-Sung Park and Kyoung J. Lee*

National Creative Research Initiative Center for Neuro-dynamics and Department of Physics, Korea University, Seoul 136-701, Korea

(Received 5 September 2005; revised manuscript received 11 May 2006; published 23 June 2006)

In this paper, we summarize our experimental observations on complex-oscillatory spiral waves that arise in a Belousov-Zhabotinsky (BZ) reaction-diffusion system. The observed wave structures generically bear *line defects* across which the phase of local oscillation changes by a multiple of 2π. The local oscillation at every spatial point along a line defect of period-2 (P-2) oscillatory media is period-1 (P-1) oscillatory. For the homogeneous BZ reaction can be excitable, simply periodic, complex periodic, or chaotic as the control parameters are tuned, a number of different complex wave states are revealed. A two-dimensional phase diagram, which includes domains of P-2 oscillatory spirals, intermittently breathing spirals, period-3 (P-3) oscillatory spirals, two different types of mixed-mode periodic spirals, and line-defect-mediated turbulence, is constructed. Several different transitions among different dynamic states are described systematically. In all cases, line defects are found to play an important role.

DOI: 10.1103/PhysRevE.73.066219 PACS number(s): 05.45.−a, 82.40.Bj, 89.75.Kd

I. INTRODUCTION

As a generic feature of diffusively coupled reactive media, spiral waves have been studied in a variety of different physical, chemical, biological, and mathematical model systems. Examples are ubiquitous in nature, ranging from several different nonlinear chemical reactions [1–11], aggregating populations of slime molds [12–16], intracellular calcium waves in oocytes [17], cardiac tissues [18–26], to brain slice preparations [27–29]. There has been much interest in these wave structures since they are universal feature of oscillatory media in general. They are also considered as a starting point in understanding general rules governing nonequilibrium pattern dynamics. Moreover, understanding their various properties have immediate implications in the related issues of biology. Although a large body of literature exists on this subject, we find that past studies have been mostly focused on spiral waves that form in either excitable or simply [i.e., period-1 (P-1)] oscillatory media.

A series of recent numerical simulation studies by Goryachev *et al.*, however, has gone beyond these popularly studied parameter regimes deeper into complex-oscillatory states. As a result, they have found a host of new interesting structures—complex-oscillatory spiral waves. While most previous studies have used generic two-species models like the FitzHugh-Nagumo equation for simplicity [9,30–33], Goryachev *et al.* have employed nonlinear model systems having three state variables therefore to make various complex oscillations become possible [34–39]. One of their earlier findings, namely, a P-2 oscillatory spiral wave in a Willamowski-Rössler reaction-diffusion model system, is reproduced in Fig. 1(a). The used model is $\frac{\partial \vec{c}(\vec{r},t)}{\partial t}=\vec{R}[\vec{c}(\vec{r},t)]+D\nabla^2\vec{c}(\vec{r},t)$, where $\vec{c}(\vec{r},t)$ is the concentration vector, D is the diffusion coefficient, and $\vec{R}[\vec{c}(\vec{r},t)]$ describes the local reaction kinetics: $dc_x(t)/dt=\kappa_1 c_x-\kappa_{-1}c_x^2-\kappa_2 c_x c_y+\kappa_{-2}c_y^2-\kappa_4 c_x c_z+\kappa_{-4}$, $dc_y(t)/dt=\kappa_2 c_x c_y-\kappa_{-2}c_y^2-\kappa_3 c_y+\kappa_{-3}$, $dc_z(t)/dt=-\kappa_4 c_x c_z+\kappa_{-4}+\kappa_5 c_z-\kappa_{-5}c_z^2$, where $\kappa_{\pm i}$ are the rate constants. The rate constants are fixed to be: $\kappa_1=31.2$, $\kappa_{-1}=0.2$, $\kappa_{-2}=0.1$, $\kappa_3=10.8$, $\kappa_{-3}=0.12$, $\kappa_4=1.02$, $\kappa_{-4}=0.01$, $\kappa_5=16.5$, and $\kappa_{-5}=0.5$. Only κ_2 is varied as a control parameter. Numerical simulations are conducted with a forward Euler method (D

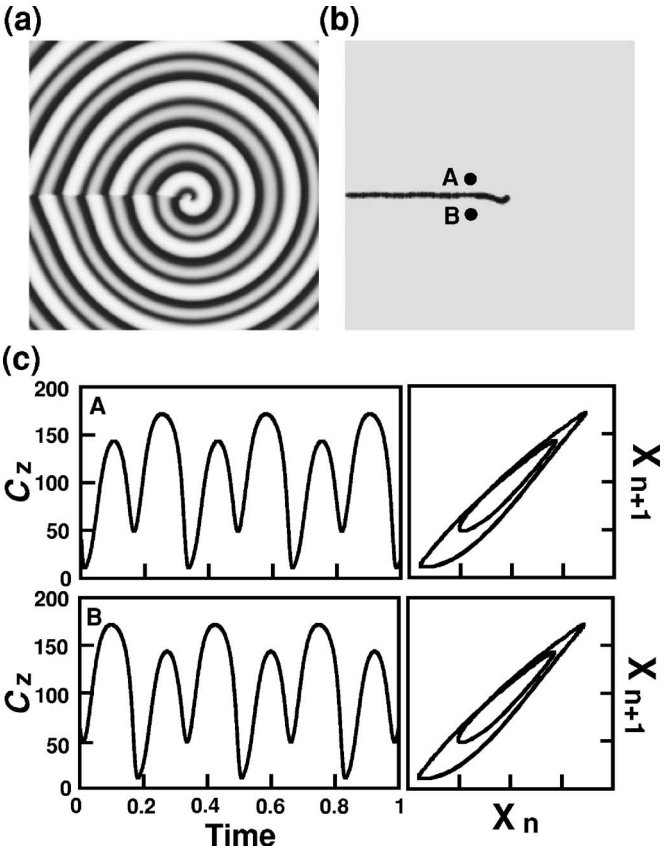

FIG. 1. Single P-2 oscillatory spiral wave in a Willamowski-Rössler reaction-diffusion system: (a) gray-scale snapshot image visualizing the scalar field C_Z; (b) a processed image revealing the underlying line defect (black line) of (a), $\kappa_2=1.53$; (c) local time series acquired at two neighboring points **A** and **B** near the line defect and the corresponding time-delayed maps. The image processing scheme associated with the frame in (b) is explained in Sec. II.

*Electronic address: kyoung@nld.korea.ac.kr

$=0.1\Delta t=10^{-3}$) in a disk domain of radius 256 using no flux boundary condition.

In its simple P-1 oscillatory regime, the model system can sustain a typical P-1 oscillatory spiral wave that rotates regularly around its core. An interesting question is then what will happen to this regular spiral wave as the homogeneous kinetics (i.e., local dynamics) undergoes a period-doubling bifurcation. The answer is now well established: the initial P-1 spiral wave transforms to a P-2 oscillatory spiral wave as depicted in Fig. 1. As this unusual spiral structure rotates about its core, a sequence of waves with two alternating amplitudes emanate from the core in succession. The local time series shown in Fig. 1(c) clearly supports the existence of these two alternating peaks. The most notable feature that distinguishes this P-2 oscillatory spiral wave from a regular P-1 oscillatory spiral wave is the existence of line defect, as shown in Fig. 1(b). The black line structure that connects the core to the boundary of the system is revealed by processing a sequence of snapshot raw images (details in Sec. II D)—the black (white) marks the area in which P-1 (P-2) oscillation takes place.

From the viewpoint of local dynamics, an interesting situation arises as one approaches this line defect from above or from below. The local time series [Fig. 1(c)] acquired at two neighboring locations **A** (above the line defect) and **B** (below the line defect) both exhibit an almost identical copy of P-2 oscillation. However, they are out of phase by a factor of 2π. By crossing the line defect, say from **A** to **B** or vice versa, the local oscillation slips rather rapidly over a short distance by an amount of 2π. Roughly speaking, at the middle point in between **A** and **B**, the two loops of corresponding P-2 cycle merge and swap their positions. Right at this spatial point, the local dynamics becomes P-1 oscillatory. The line defect is nothing but a collection of such points being continuously connected in space forming a line. Since the local dynamics on the line defect is P-1, the structure can be viewed as a defect in an otherwise P-2 oscillatory bulk medium.

Sometime before the first computational demonstration of a P-2 spiral wave by Goryachev *et al.*, Yoneyama *et al.* [40] reported an unusual Belousov-Zhabotinsky (BZ) spiral wave that closely resembles the P-2 oscillatory spiral wave of Goryachev's model system in many respects. In their paper, however, the authors concluded that the observed wave structure was made possible by the oxygen gradient along the z axis. This finding was also modeled successfully by a simplified three-species Oregonator model having a z gradient of a stoichiometric factor [41].

In an attempt for studying complex-oscillatory wave structures systematically in a real laboratory experiment, we have developed a two-side, continuously fed, open gel reactor employing a BZ reaction in which wave patterns can be created and maintained for a long period of time almost indefinitely. We have systematically explored various parameters of our experimental system: the chemical composition of the pattern forming gel medium and its thickness, as well as the concentrations of various input reactants and the flow rates, were varied to achieve a complex-oscillatory state within the gel medium [42–44]. Our experimental system has proven to be very fruitful. Over the last several years, we have found a variety of different complex wave structures, including P-2 spiral waves, P-3 spiral waves, two different mixed-mode waves, and spatiotemporally chaotic states. All of these complex wave structures involve line defects and many details are found to be a quite general property of any complex-oscillatory media. In this paper, we shall discuss those properties and various transitions among different wave states.

Our paper is organized as follows. In the next section we describe our experimental methods including the design of two-side fed gel reactor. In Sec. III we describe different types of complex-oscillatory wave states that are found and present a comprehensive phase diagram. We discuss the emergence of a P-2 spiral wave from an initial P-1 spiral wave and the subsequent transitions in Sec. IV. The transverse instability of line defect associated with a P-2 spiral wave and two subsequent transition to the so-called line-defect mediated turbulence (LDT) are discussed in Sec. V. We then proceed to the emergence of mixed-mode periodic spiral waves having two different domains, each having a different period in Sec. VI. In Sec. VII, period-three oscillatory spiral wave dynamics are discussed. Finally, we summarize our results and discuss several interesting issues in Sec. VIII.

II. EXPERIMENTAL SYSTEM

For long-term controlled experiments on nonlinear chemical waves, it is quite crucial to establish an appropriate reactor—a spatially extended open system, where a time-asymptotic pattern can be sustained for a fixed set of parameter values and where patterns can be controllably changed by adjusting parameter values. Here, in this section we describe the overall design of our reactor, the chemical composition and physical dimensions of the porous gel medium in which patterns are sustained, the pump system for delivering chemical reactants, and finally, the optics and image acquisition system.

A. Two-side fed gel reactor

Our rector is composed of a thin composite slab of porous medium and two reservoirs that are constantly replenished with a mixture of reagents. Figure 2 schematically depicts the design of our reactor which is modeled after the chemical reactor developed earlier by Ouyang *et al.* for studying Turing patterns [45]. A major difference between the two is that here the pattern forming medium is a composite slab of a polyacrylamide gel membrane (0.6 mm thick, 22 mm diameter) instead of a Vycor porous glass disk. The gel membrane is structurally supported by an Anopore disk (0.2 μm pore size, 0.16 mm thick, Whatman) and backed by a nitrocellulose membrane (0.47 μm pore size, 0.16 mm thick, Whatman) that serves as a visual background. The Anopore disk has an array of micro holes with no lateral connectivity, and here it is used only for a structural support of the soft gel medium. The nitro-cellulose membrane is used as an imaging background. Since the porosity of this membrane is rather high and its thickness is very thin, the residence time

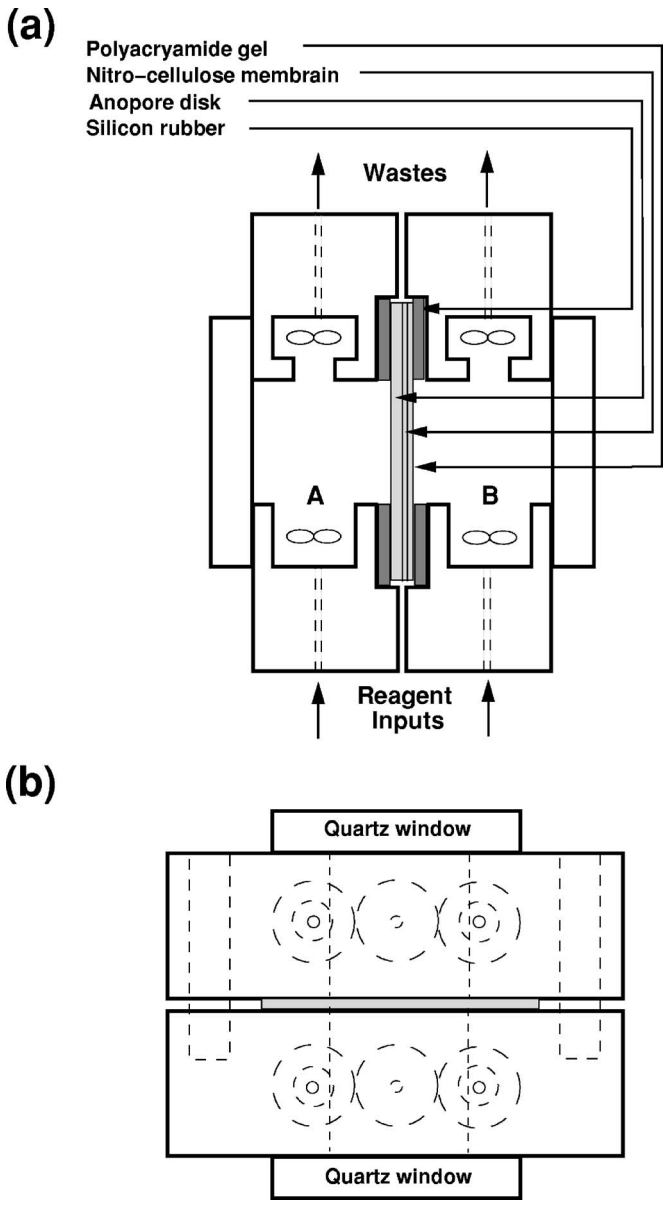

FIG. 2. Schematic diagrams of the two-side fed gel reactor: side view in (a) and top view in (b). The reactor is basically a thin composite slab of porous medium sandwiched between two reservoirs of chemical reactants.

of the reagents within this membrane is negligible compared to that in the gel. The gel medium that is inert to the chemical reaction guarantees the necessary reaction-diffusion condition.

The composite slab is sandwiched between two reservoirs of reagents. For effective mixing of reagents in the reservoir, each reservoir is stirred continuously using three small magnetic bars (two at the top and one at the bottom). The reactor parts are machined with Plexi-glass and Teflon. The optical windows on each sides are quartz.

B. Composite gel medium

The gel is prepared as following. First, the following gel solutions are mixed thoroughly in a small beaker: 2.5 ml of acrylamide solution (20 g per 100 ml, Sigma), five drops of N, N′-methylene-bis-acrylamide (0.5 g per 25 ml, Sigma), and three drops of ammonium persulfate (2 g per 10 ml, Sigma). Then, two drops of cross-linking agent triethanolamine (3 g per 10 ml, Sigma) is added to the mixture to initiate polymerization. This polymerizing solution is then poured onto a double layer composed of a nitro-cellulose membrane and an Anopore disk that are placed on a thick glass plate. The double layer is presoaked with the mixed gel solution not containing triethanolamine. The poured gel solution is then covered by another glass plate at a proper stage of the polymerization. Thus the acrylamide gel is impregnated into the membranes. The thickness of the composite gel slab is controlled by using a pair of two standard shims (0.6 mm thickness). As the polymerization is completed, the composite gel slab is cut and trimmed around the boundary of Anopore disk. The composite gel membrane is then soaked in distilled water for several hours before usage.

At the very initial stage of developing our BZ reactor, we tried three different gel thicknesses (0.55, 0.60, and 0.65 mm). In all cases, we were able to produce P-1 and P-2 oscillatory spiral waves. However, we found that the thickness of 0.6 mm gave the best image contrast over the other two cases and fixed the gel thickness to be 0.6 mm thereafter—the gel thickness is in no way a good control parameter for changing it can influence the gradients of every chemical that is involved. Reducing the thickness of gel slab further was inadequate to guarantee the the visualization of waves and stable mechanical rigidity.

C. BZ solutions and delivery system

The BZ reaction used in our system has malonic acid as the organic species and ferroin [a complex of iron and (1, 10) phenanthroline] as the catalyst. The BZ reagents are grouped into two and fed to the reservoirs, one on each side of the gel slab. Each reservoir of chemicals is not chemically reactive by itself, and the reaction takes place only when the diffused chemical reagents are met within the gel slab. We have used the input concentrations of sulfuric acid $[H_2SO_4]$ and sodium bromate $[NaBrO_3]$ as the control parameters, while the concentrations of the others are fixed. Sulfuric acid $[H_2SO_4]$ and sodium bromate $[NaBrO_3]$ are supplied to one reservoir, while malonic acid $[CH_2(COOH)_2]=0.53$ M, ferroin $[Fe(phen)_3^{2+}]=2.5$ mM, sodium bromide $[NaBr]=0.1$ mM, and sodium dodecyl sulfate $[SDS]=0.1$ mM are supplied to the other reservoir.

The chemical reagents are delivered to the reservoirs using four precision piston pumps (P-500, Pharmacia) as illustrated in Fig. 3. Each reservoir has a volume of 10 ml and is magnetically stirred by three magnetic stirrers. The reagents fed to the reservoir A are pre-mixed as shown in Fig. 3. The flow rate is fixed at 120 ml/hr and the reactor temperature is regulated at 22.0 ± 0.2 °C using a cooling chamber. As the boundary conditions at two surfaces are not identical, concentration gradients exist across the gel thickness. In the plane perpendicular to the gradient, however, the system is homogeneous at least at the gel surfaces.

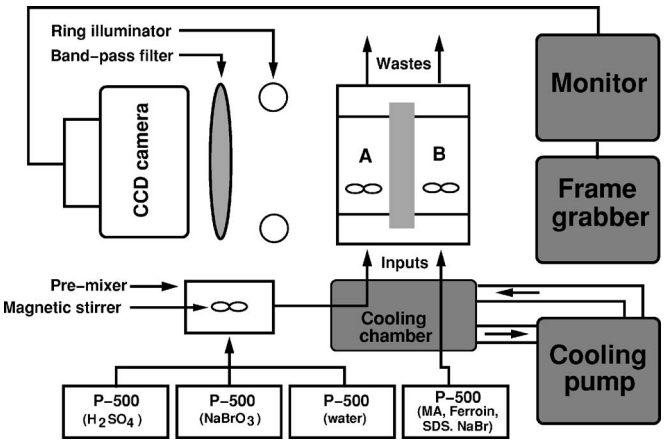

FIG. 3. Schematic illustration of our experimental setup that includes a gel reactor, four precision piston pumps and a premixer, coolant circulation unit, and an image acquisition system.

D. Image acquisition and processing method

Raw images are acquired at the spatial resolution of 480 $\times 640$ using a charge coupled device (CCD) camera (XC-77, Sony) and a frame grabber (Meteor, Matrox). The wave patterns are illuminated by a 100-W halogen lamp through a fiber optic ring illuminator. As illustrated in Fig. 3, images are captured in a reflective mode. The difference of the light absorption spectra of ferroin and ferriin is the greatest at the wavelength of 480 nm, and subsequently, we have used a narrow band-pass filter (peak wavelength 480 nm, bandwidth 30 nm) to maximize the image contrast. In this imaging modality, the reduced complex (ferroin) appears dark while the oxidized complex (ferriin) appears bright.

In order to reveal the line defects that underlie the morphology and the dynamics of P-2 oscillatory spiral waves, we have formulated the following scalar field: $\Delta V(\vec{r},t) = \frac{1}{\tau}\int_0^\tau |V(\vec{r},t+t') - V(\vec{r},t+\tau+t')| dt'$. Here, $V(\vec{r},t)$ represents the gray scale values of the individual pixels in the raw images. τ is the period of P-1 oscillation just before the P-1 to P-2 transition. Technically, it is determined to be the arithmetic average of τ_1 and τ_2, where τ_1 and τ_2 are slightly detuned two periods of P-2 time series. When the scalar field ΔV is rendered as a black-and-white image, the area exhibiting P-1 oscillation should appear very dark ($\Delta V = 0$) while non-P-1 oscillatory areas should appear bright ($\Delta V \gg 0$).

A clear example of a P-2 oscillatory spiral wave having a line defect (black line) is given in Fig. 1(b). In this particular case, the P-1 oscillatory domain shows up as a form of line connecting the spiral core to the boundary. On the other hand, the remaining bulk medium (white) executes a P-2 oscillation as the spiral rotates fanning out waves. The black line structure is thus termed as a line defect. When the medium is composed of several different domains, each having a different periodicity, one can clearly distinguish them in the gray scale image of ΔV. This will be further discussed in later sections. The image of scalar field ΔV is in fact a very useful tool for analyzing complex-oscillatory wave states in general.

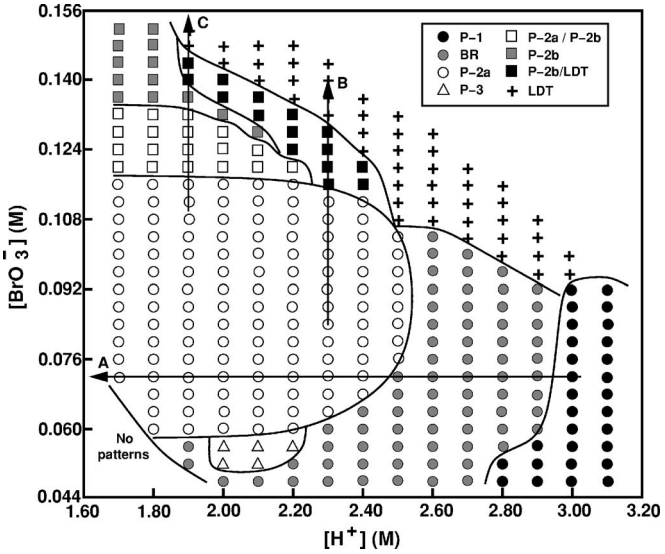

FIG. 4. Phase diagram of complex-oscillatory (spiral) waves in a BZ reaction-diffusion system: P-1 spiral wave (P-1), two different types of P-2 spiral wave (P-2a and P-2b), intermittently breathing spiral wave (BR), P-3 spiral wave (P-3), two different types of MMP spiral waves (P-2a/P-2b and P-2b/LDT), and LDT. The solid lines separating different periodic states are schematically drawn to guide the eyes. Transitions among various states are discussed following three arrow-head tracks (A, B, and C). The parameters are scanned at the resolution of 0.1 M for $[H_2SO_4]$ and 0.004 M for $[NaBrO_3]$.

III. PHASE DIAGRAM

The history of spiral waves traces back to early 1970 when they are first seen in a BZ system [1,2]. Ever since, so many different issues have been addressed regarding them through many experiments and computer simulations, and theories [3–6,48]. Interestingly, however, previous studies are mostly concerned with phenomena that are associated with excitable or simply oscillatory (P-1) kinetics, and only a few recent studies discuss wave dynamics in parameter regimes that are associated with more complex oscillations [49–55]. Experiments on the popularly studied BZ chemical waves are no exception. Chemical waves have been studied in various parts of multidimensional parameter space. Yet, previous studies on BZ spiral waves have mostly been conducted in excitable or simply periodic regimes and there is still a large parameter space that has not been explored. By all means, it is a well established fact that BZ chemical reaction can produce a variety of different complex-periodic temporal oscillations including deterministic chaos when prepared in a continuously fed homogeneous (stirred) reactor [30,56–66].

Here, we present a phase diagram illustrating various types of complex-oscillatory spiral waves that have been acquired in our BZ reaction-diffusion system over the last several years (see Fig. 4). The phase diagram is constructed with two control parameters, $[H^+]$ and $[BrO_3^-]$, to which the wave dynamics is quite sensitive. In addition to the conventional P-1 oscillatory spiral wave, seven different complex-oscillatory spiral waves are observed. They are intermittently

breathing spiral wave, P-2a and P-2b spiral wave, P-3 spiral wave, two different types of MMP spiral wave, and spatiotemporal chaos.

Period-1 oscillatory regular spiral waves, which are popularly reported in many other experiments, are observed in a high $[H^+]$ regime of our phase diagram. In this regime, one sees P-1 oscillatory wave trains emanating out continuously from spiral cores as they rotate steadily. Accordingly, the local time series obtained at a fixed location is P-1 oscillatory [Fig. 5(a)] everywhere except for the cores.

The input concentration $[H^+]$ is found to be a key parameter that brings a P-1 oscillatory spiral wave to a P-2 spiral wave. The transition comes in two steps along the path **A** in the phase diagram of Fig. 4. As $[H^+]$ is lowered, regular P-1 spirals lose their stability by allowing occasional "2π phase slips"—this will be discussed in detail in the next section. During these slips, the profile of the original P-1 spiral is unchanged while its thickness is "breathing." Therefore one may state that the P-1 spiral waves lose their stability first in time domain only yielding the breathing spiral waves (BR). When $[H^+]$ is lowered further, the 2π phase slips become more frequent and every second spiral rotation becomes a small-amplitude excitation or omitted completely [see Fig. 5(c)]. Consequently, a P-2 oscillatory spiral wave (P2-a) ensues. The P-2a spiral wave has a spiraling line defect that cuts through the original P-1 spiral wave. Therefore the P-2a spiral wave is wavelength-doubled in space as well as period-doubled in time.

As the value of $[H^+]$ is further lowered, the P-2a spiral waves become unstable and destabilize. In this very low $[H^+]$ regime, the system no longer supports any waves. Within the stable P-2a spiral wave regimes, we have found a number of interesting transitions of line defect that are to be discussed in Sec. IV. In a very small parameter regime of low $[H^+]$ and low $[BrO_3^-]$, spiral waves having P-3 temporal dynamics are also observed [Fig. 5(d)]. These P-3 spiral waves have a complex line defect that is highly nontrivial.

As $[BrO_3^-]$ is increased, P-2a spiral waves become spatiotemporally chaotic in two different ways. First, P-2 oscillatory spiral waves become unstable via a transverse instability of line defects (along the path **B** in the phase diagram of Fig. 4). The other type is mediated by mixed-mode periodic (MMP) spiral waves (along the path **C**). Transitions arising along the two different paths will be discussed in detail in Secs. V and VI, respectively. The spatiotemporally chaotic state revealed in our BZ system is characterized by a fast and erratic motion of line defects thus termed line defect mediated turbulence (LDT). In this state, small wave segments with irregular shapes constantly appear and decay, and its local time series obtained at a fixed location does not show any discernible periodicity [Fig. 5(e)].

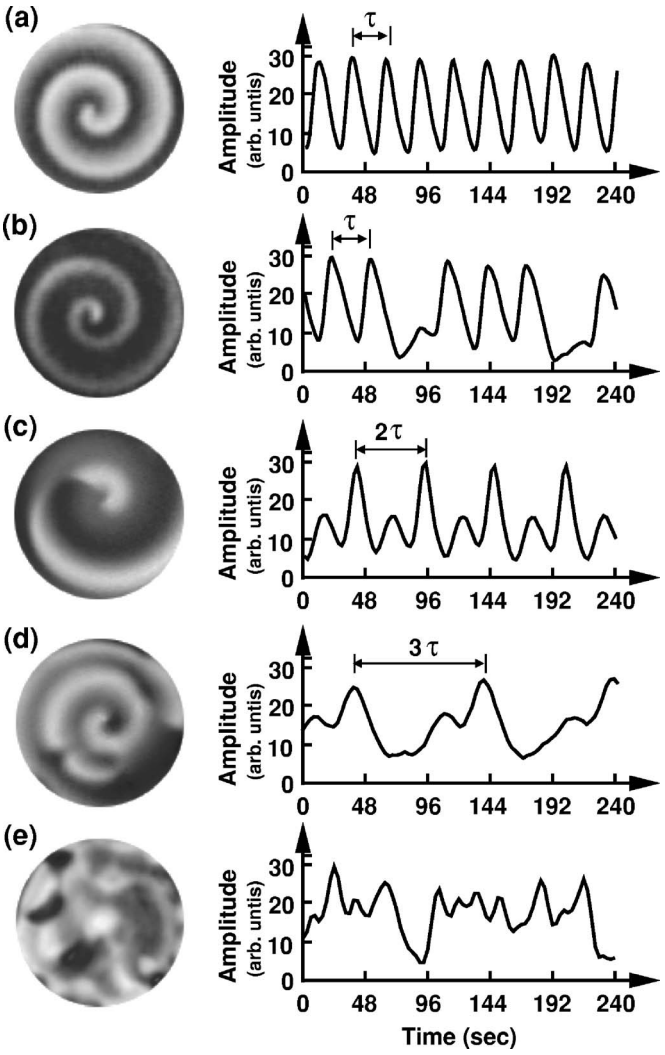

FIG. 5. Snapshot images of BZ spiral waves revealed in our BZ experimental system: (a) typical P-1 spiral wave with its typical local time series, $[H^+]=3.02$ M and $[BrO_3^-]=0.075$ M; (b) intermittently breathing spiral wave and its local time series having occasional 2π phase slips, $[H^+]=2.78$ M, $[BrO_3^-]=0.075$ M; (c) discontinuous P-2 spiral wave with a line defect and its regular P-2 local time series, $[H^+]=2.32$ M, $[BrO_3^-]=0.083$ M; (d) discontinuous P-3 spiral wave with a line defect and its regular P-3 time series, $[H^+]=2.10$ M, $[BrO_3^-]=0.060$ M; (e) fully developed line defect turbulence and its chaotic local time series, $[H^+]=2.32$ M, $[BrO_3^-]=0.132$ M. In the raw images (a)–(e), white and black represent the oxidized and reduced states, respectively. The τ in the local time series of (a)–(d) is a period of a fundamental P-1 oscillation. The diameter of the viewing area is 3.2 mm.

IV. ONSET OF A P-1 TO P-2 SPIRAL WAVE TRANSITION AND BEYOND

The P-1 to P-2 spiral wave transition is investigated by decreasing $[H^+]$ along path **A** of the phase diagram. As briefly mentioned in the previous section, this transition takes place in two different steps. The first step is the transformation of the regular P-1 oscillatory spiral wave of Fig. 6(a) to the P-2 oscillatory spiral wave of Fig. 6(b) having a spiraling line defect. Subsequent to this transition, the initial spiraling line defect dilates and the continuity of the initial P-1 spiral wave is lost. As a result, the spiral wave becomes P-2 both in space and time [Fig. 6(c)]. The dilated line defect rotates slowly in the same direction of spiral wave rotation. Quite interestingly, we have observed that the rotating line defect exhibits a meandering transition which is quite similar

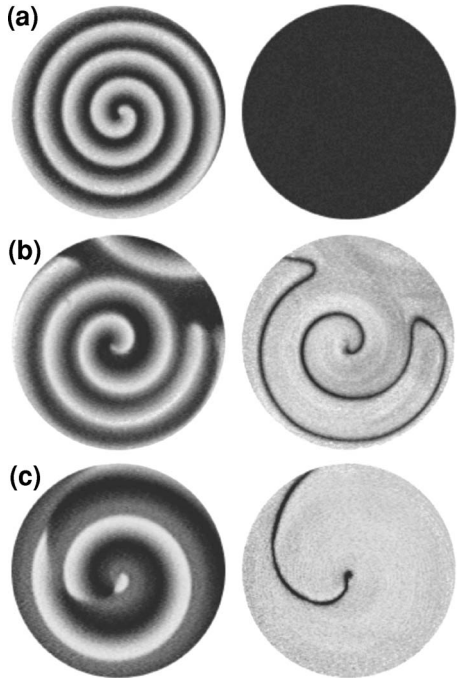

FIG. 6. Snapshot images of BZ spiral waves (left) and the corresponding images of a line defect (right): (a) P-1 spiral wave with no line defect, $[H^+]=3.02$ M; (b) continuous P-2 spiral wave and the associated line defect having the same shape of a P-1 spiral, $[H^+]=2.40$ M; (c) discontinuous P-2 spiral wave and the associated line defect having a line defect with a shape different from the P-2 spiral wave of (b), $[H^+]=2.12$. The diameter of the viewing area is 8.2 mm. As in Fig. 1, in the processed image of P-1 domain (i.e., line defect) appears black ($\Delta V=0$) and the bulk P-2 domain appears bright. The spiraling line defect in (b) is folded due to the interaction with a neighboring spiral wave.

to that of a P-1 oscillatory spiral wave, a topic of extensive previous investigations [67–71]: The tip of the line defect initially rotates around a small circle with a well-defined period, then undergoes a Hopf bifurcation acquiring an additional circular orbit to create a compound orbit. In this section, we discuss these three different transitions in detail.

A. Emergence of the breathing line defect at the onset

In our experimental system, spiral waves spontaneously form during the early stage when BZ chemical reagents are just fed into the gel membrane through diffusion. In the high $[H^+]$ regime, the system produces a simply periodic P-1 spiral wave as shown in the left frame of Fig. 6(a). This spiral wave has no defect except for the topological singularity at the core. Thus the processed image on the right-hand side rendering the scalar field ΔV in gray scale shows no structure at all.

As $[H^+]$ is lowered, however, the simple P-1 oscillatory spiral wave becomes unstable as shown in Fig. 7. When $[H^+]$ reaches about 2.80 M, the initial P-1 spiral wave starts to modulate every now and then—i.e., the width of the spiral wave changes in time as it rotates. An example is depicted in Fig. 7. When the initial spiral wave ($t=0$) rotates, its width

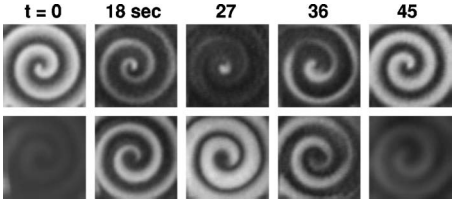

FIG. 7. Sequential images of a breathing spiral wave at the P-1 to P-2 spiral transition (top row) and the corresponding images of a *breathing* line defect (bottom row). The breathing line defect appears whenever a local P-2 episode [arrows in Fig. 8(b)] interrupts an otherwise P-1 oscillation. The width of the spiraling line defect changes as a P-2 episode sweeps through in a time series. The processed images show the scalar field ΔV. The image size is 6.4 mm^2 and $[H^+]=2.80$ M.

gradually shrinks and vanishes completely (except for a very small piece at the core) by the time it completes a full rotation ($t=27$ sec). Then, the spiral wave regains its thickness or re-emerges during the next cycle of rotation ($t=36-45$ sec). The integrity of the initial P-1 spiral is unchanged during this breathing event. Initially, this breathing episode arises sparsely and randomly. But they occur more frequently as $[H^+]$ is lowered further, and eventually the breathing comes into the system once for every two cycles. Figure 8, which summarizes the spiral wave activities with (one-dimensional) space-time raster plots and corresponding local time series, depicts the whole situation quite clearly.

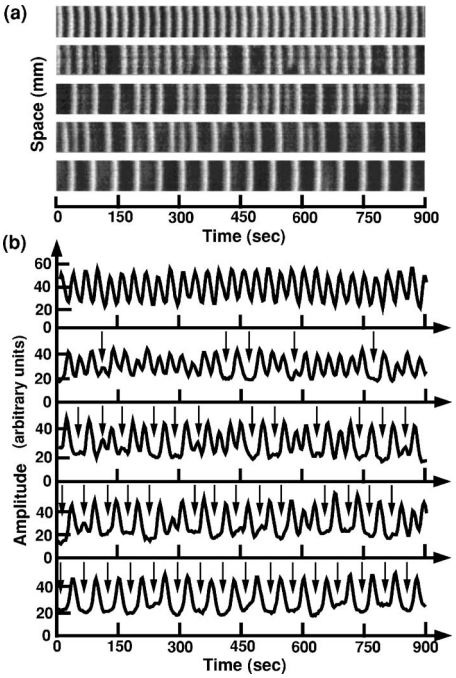

FIG. 8. Intermittent behaviors during a P-1 to P-2 spiral wave transition in space (a) and time (b). The space-time plots and local time series are obtained from different values of $[H^+]$ (from top to bottom, $[H^+]=3.02$, 2.80, 2.60, 2.48, and 2.40 M). The y axis of (a) represents a straight line segment (3 mm) in the perpendicular direction of wave propagation. The arrows in (b) mark the positions where 2π phase slips take place.

At $[H^+]=3.02$ M, the system supports a P-1 oscillatory spiral wave. Therefore the corresponding wave train of Fig. 8(a) (top frame) and the local time series of Fig. 8(b) (top frame) are P-1 oscillatory. At $[H^+]=2.80$ M, the initial P-1 wave train experiences occasional 2π phase slips as marked by arrows. We note that there is some gradual amplitude modulation when the signal switches from a P-2 episode to the following P-1 oscillation, or vice versa. Therefore the signal appears more complex than a simple mixture of P-1 and P-2 signals. As the value of $[H^+]$ is lowered further, the number of P-2 episodes increases gradually. Eventually one out of every two successive peaks becomes lost by the time at $[H^+]=2.40$ M [see the second frame through the fifth frame in Fig. 8(a) and the corresponding time series in Fig. 8(b)]. In other words, the initial P-1 oscillatory system has period-doubled to a P-2 state. Note that since this transition takes place over a finite range of $[H^+]$, the period of the P-2 signal is not exactly equal to twice the period of the initial P-1 oscillation.

In connection with the P-1 line defect of P-2 oscillatory spiral waves, one can view the phenomenon discussed above being driven by the existence of a *breathing* line defect which has the same spatial profile of a P-1 spiral wave. Unlike the regular P-1 line defect, the breathing line defect emerges only when there arises a P-2 episode. It is termed as "breathing," because its thickness changes in time as illustrated in the sequence of processed images in the bottom row of Fig. 7. During the whole process of an initial P-1 spiral wave becoming a P-2 spiral wave via a stage of breathing intermittent spiral wave, the property of underlying line defect changes as well: its breathing activity gradually comes to an end yielding a thin *static* line defect having the same shape of a P-1 spiral as the system reaches to the P-2 oscillatory regime [see Fig. 6(b)].

Here, we note that the observed transition has a very strong analogy to the phase synchronization-desynchronization transition, often called eyelet intermittency generically occurring in systems of two-coupled nonlinear oscillators [72–74]. The transition shows rare and intermittent 2π phase slips near the onset and frequent and regular 2π phase slips away from the onset. In our experimental system, the observed P-2 episodes in an otherwise P-1 signal can be considered as 2π slips mediating the transition of a P-1 spiral to a P-2 spiral.

Note that the snapshot image of a P-2 oscillatory spiral wave of Fig. 6(b) having a static line defect—the thin black contour that exactly matches the profile of the associated spiral wave on the left—appears not at all different from a regular P-1 spiral wave. Therefore one may claim that the spiral wave of Fig. 6(b) is temporally P-2 (except along the line defect) but spatially P-1. The emergence of line defect in a form of P-1 spiral is quite unexpected for the previous model simulation results all have shown either straight (Rössler system) [36] or irregular (Willamowski-Rössler system) [34,35] line defects only.

B. Dilation of a spiraling line defect

When $[H^+]$ becomes about 2.32 M, the static line defect shown in Fig. 6(b) is no longer stable and it starts to dilate to acquire a much larger pitch than that of the associated spiral wave as shown in Fig. 6(c). Consequently, the line defect intersects with the spiral wave breaking its continuity. As a result, the spiral wave acquires the spatial periodicity of 2 (i.e., the wavelength is doubled) in addition to the temporal periodicity of 2. In this regard, the P-2 spiral of Fig. 6(c) distinguishes itself from the one shown in Fig. 6(b) that retains the spatial periodicity of 1.

The dynamical process of unwinding line defect is nontrivial as discussed in our previous paper [43]. Following a decrease in $[H^+]$, the unwinding process starts from the spiral core region and advances radially outward—the pitch of the line defect modulates in space and time. Moreover, neighboring line defects often collide and annihilate each other to produce two cusp structures. Subsequently, the cusps travel away from each other dilating the spiraling line defect. The nexus of complex unwinding, annihilation, and dilation process keeps on until a new regular line defect is established. Although the resulting line defect [Fig. 6(c)] is smooth and regular, the ones for the parameter range between Figs. 6(b) and 6(c) are in general quite irregular and unsteady.

C. Meandering and drift transitions of a line defect

In contrast to the static line defect shown in Fig. 6(b), the dilated line defect of Fig. 6(c) is dynamic. It rotates steadily like a rigid body in the same rotational direction of the spiral wave, as illustrated in Figs. 9(a) and 9(b). The dark black circle in the inset of Fig. 9(a) [and in Fig. 9(b)] represents the orbit traced by the tip of line defect. The rotation of the line defect around this black circular orbit is rather slow ($\omega_1=3.8$ rad/h): roughly 156 times slower than that of the associated spiral wave ($\omega_0=594$ rad/h). In fact, there are two different circular orbits associated with the P-2 spiral wave shown in Fig. 9(a): the black circle (radius, $r_1=0.4$ mm) traced by the tip of line defect and the white circle ($r_0=0.1$ mm) traced by the tip of spiral wave [75]. In fact, the spiral wave shown in Fig. 9(a) is a meandering P-2 oscillatory spiral wave whose core executes a epicycloid motion involving two coupled circular motions with radii r_0 and r_1 and two frequencies ω_0 and ω_1.

Meandering spiral waves have been a topic of numerous studies over the last 20 years or so [67–71], but all of them were concerned about the meandering behavior of P-1 oscillatory spiral waves. Here we just discussed that some P-2 oscillatory spiral wave can meander very much like a meandering P-1 spiral wave. The most fascinating part is, however, yet to be explained.

Following a small decrease in the input $[H^+]$, the simply rotating line defect of Fig. 9(b) undergoes a Hopf bifurcation resulting in a compound orbit of Fig. 9(c). This orbit, formed by two combined circular motions, is a hypercycloid: the primary circle (radius r_1, angular frequency ω_1) orbits the secondary circle (radius r_2) with a new rotation period ω_2 and spins about its center in the same direction. As a consequence, the motion of rotating spiral wave now involves three distinct frequencies and accompanying three different radii.

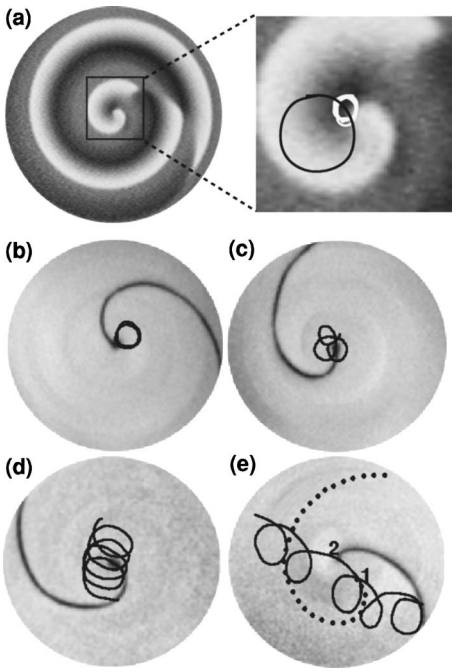

FIG. 9. Meandering transition and drift of a spiraling line defect. (a) typical P-2 spiral wave having a simply rotating spiraling line defect ($[H^+]=2.22$ M); (b)–(e) processed images of ΔV in gray scale revealing the underlying line defect [from (b) to (e), $[H^+]=2.22$, 2.12, 2.04, and 1.94 M, respectively]. (b) shows a simply rotating line defect of the P-2 spiral wave shown in (a), (c) is a line defect whose tip meanders around a hypercycloid orbit ($r_1=0.4$ mm, $\omega_1=3.4$ rad/h, $r_2=0.3$ mm, $\omega_2=0.7$ rad/h), and (d) and (e) are a rotating line defect with a net drift [for (d), $r_1=0.7$ mm, $\omega_1=3.1$ rad/h, r_2 and ω_2 undetermined, and for (e), $r_1=0.8$ mm, $\omega_1=5.6$ rad/h, r_2 and ω_2 undetermined]. The inset of (a) is a blown-up image of the core region. The white circular orbit (drifting very slowly around the black circle) in the inset of (a) is the passage traced by the tip of P-2 oscillatory spiral wave. The saturated black lines are the orbits traced by the tip of line defects. The dotted line in (e) is drawn to represent the profile of line defect at the marked location **1**. The rotation frequency Ω of the associated spiral waves themselves is 594 rad/h for (a) and (b), 552 rad/h for (c), 528 rad/h for (d), and 500 rad/h for (e). The diameter of the viewing area is 8.2 mm.

The shape of compound orbit traced by the tip of line defect is quite sensitive to the control parameter $[H^+]$. When $[H^+]$ is decreased less than a few percent from that of Fig. 9(c), r_2 rapidly diverges to infinity and ω_2 becomes very small. Nevertheless, the values of r_1 and ω_1 both change less than 50%. As a consequence, a net drift motion appears as shown in Fig. 9(d). The drift becomes more eminent when $[H^+]$ is further lowered as shown in Fig. 9(e). Here, we note that the shape (or mean curvature) of line defect is not steady but oscillates periodically as its tip moves on the compound orbit. The line defect with the maximum (or minimum) curvature reaches at the location marked by **1** (or **2**) as indicated in Fig. 9(e). All these observations are remarkably similar to the well known phenomena of meandering spiral wave in excitable or P-1 oscillatory media. However, epicycloid motions are yet to be observed.

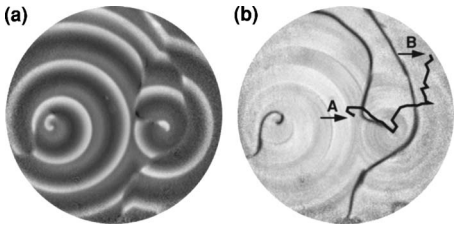

FIG. 10. Erratically drifting P-2 spiral waves (a) and the corresponding processed image of line defects (b). The tip trajectory of line defect [solid line: from $\mathbf{A}(t=0)$ to $\mathbf{B}(t=3600$ sec)] is superimposed in (b). The diameter of the viewing area is 18 mm, and $[H^+]=1.80$ M.

A further decrease of $[H^+]$ makes the motion of the tip of line defect very irregular as shown in Fig. 10. The line defect no longer rotates about its tip but drifts away in an erratic way: the speed of moving tip is not steady, and, subsequently, the shape of the line defect becomes quite irregular. Consequently, the system loses all spiral cores in the long run and becomes a reduced homogeneous state. These observations are visually similar to the results of model simulation recently carried out by Davidsen *et al.* [76]. However, we note that their simulation results were obtained using a chaotic Rössler model system.

V. FORMATION OF WIGGLED LINE DEFECTS AND LINE DEFECT MEDIATED CHEMICAL TURBULENCE

In this section, we summarize our previous results on the sequence of transitions along the route **B** specified in the phase diagram of Fig. 4 [44]. Locally, the line defects in P-2 oscillatory media can be viewed as a front separating two P-2 domains oscillating 2π out of phase. Here we show that the shape of these line defects can become sinusoidal by a transverse instability. This instability ultimately leads to a line defect filled chemical turbulence that is characterized by proliferation, annihilation, erratic motions of line defects.

Although the change in $[H^+]$ significantly affects the dynamics of BZ spiral waves, we find that $[BrO_3^-]$ is another key factor that can bring the system to a turbulent regime. Along the route **B**, $[H^+]$ is fixed at 2.30 M and only $[BrO_3^-]$ is increased. Our experiment has begun with a P-2 spiral wave possessing a nearly straight line defect: see the spiral wave in Fig. 11(a) and the underlying line defect in Fig. 11(c). The line defect is slightly curved and this property seems to be related to its slow rotation. In a systematic increase of $[BrO_3^-]$, we have found that the shape of the line defect transforms in a quite interesting manner: The initial, straight line defect starts to form wiggles in the transverse direction of the wave propagation and the amplitude of wiggles becomes more pronounced as the value of $[BrO_3^-]$ increases [see Figs. 11(d)–11(f)]. These wiggled line defects are quite static in their time-asymptotic (steady) states. The wiggling of the line defect is caused by a transverse instability where there are two competing influences, as discussed in Ref. [44].

When the control parameter $[BrO_3^-]$ is increased further to 0.116 M, the sinusoidal wiggle of line defect is no longer

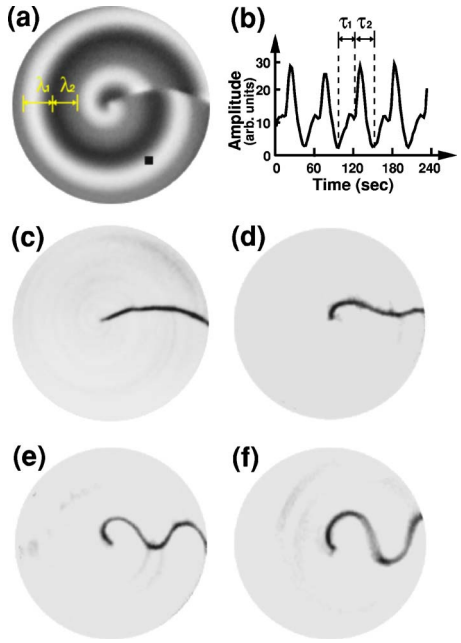

FIG. 11. (Color online) Transverse instability of the line defect of a P-2 oscillatory BZ spiral. (a) and (c) show a single P-2 spiral wave and its corresponding processed image of line defect: $[BrO_3^- -]=0.083$ M (b) A typical P-2 oscillatory local time series [taken at the position marked by the black square in (a). (d)–(f) Pseudocolor images of the scalar field ΔV revealing the underlying line defects (black line: region of $\Delta V=0$) of P-2 spiral waves for $[BrO_3^-]=0.091, 0.100, 0.108$ M respectively. $\tau=(\tau_1+\tau_2)/2$, where τ_1 and τ_2 (or λ_1 and λ_2) are the two alternating periods (wavelengths) of the P-2 spiral wave. The diameter of the viewing area is 6.4 mm.

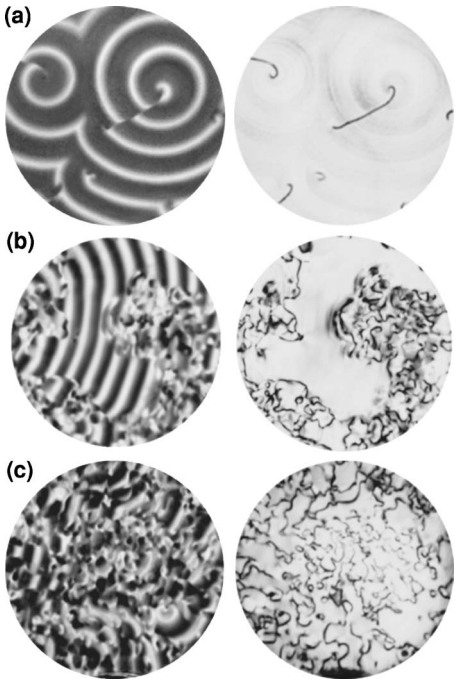

FIG. 12. Snapshot images of BZ spiral waves (left) and the corresponding processed images of line defects (right): (a) P-2 spiral waves with line defects, $[BrO_3^-]=0.106$ M; (b) a coexisting state of periodic (P-2) domain and chaotic domain, $[BrO_3^-]=0.124$ M. This chaotic domain is filled with a tangle of line defect; (c) fully developed turbulent pattern, $[BrO_3^-]=0.132$ M The diameter of viewing area is 18 mm.

stable and spatial modes smaller than $\lambda=\lambda_1+\lambda_2$ arise. Unstable wiggles deform, proliferate and break up into many pieces that again grow and evolve in an erratic fashion. Eventually, a mixed state with patches filled with a highly complex tangle of line defects forms as shown in Fig. 12(b). Within these turbulent patches irregular spiral cores (or, singular points where line defects terminate) still exist, and those that lie near the domain boundary generate periodic wave trains. The chaotic domain grows gradually at the expense of the regular periodic domain upon a further increase of $[BrO_3^-]$. Fully developed spatiotemporal chaos [Fig. 12(c)] appears around $[BrO_3^-]=0.132$ M. Note that even at this stage, line defects underlie the dynamics and morphology of the whole system.

At this point, it is perhaps worthwhile to indicate that a remarkably similar sequence of phenomena was also observed in a generic model reaction-diffusion system employing Willamowski-Rössler (WR) kinetics [44]: Just as in the BZ experiment, an initially flat line defect of a P-2 spiral wave undergoes a transverse instability forming a wiggled line defect that eventually leads to a chaotic patch formation.

In regard to the line defect turbulence discussed here, we note that a similar type of line defect turbulence was reported earlier by Goryachev *et al.* in a period-4 (P-4) oscillatory regime of a Rössler reaction-diffusion model [37] and in a chaotic regime of a WR reaction-diffusion model [77]. In their study, chaotic patches form around shock areas where waves collide and annihilate. There, line defects—Termed as Ω_2 curves—nucleate spontaneously as a form of "bubble," and proliferate producing chaotic local dynamics. In other words, the vanishing phase gradient along the shock line initiates the formation of the chaotic patches. In contrast, our line defect turbulence seems to originate from the transverse instability of existing line defects and their subsequent deformations.

VI. MIXED-MODE PERIODIC SPIRAL WAVES

Mixed-mode oscillations are a well known phenomenon observed in various nonlinear chemical and biological systems [78–81], and the Belousov-Zhabotinsky reaction is one of the best known examples [30,57,59,65,66]. This section describes a 2:3 mode-locked mixed-mode periodic (MMP) BZ spiral wave. We discuss the emergence of this particular MMP spiral wave state from a regular P-2 spiral wave state along the route **C** as specified in the phase diagram of Fig. 4. Following the same route, we also observe that the MMP spiral wave state becomes a spatiotemporally chaotic state if $[BrO_3^-]$ is further increased. Here, we explain these two transitions in detail.

A. Transition of a short period P-2 spiral wave (P-2a) to a long period P-2 spiral wave (P-2b) via 2:3 mode-locked MMP spiral wave state

Along the route **C** shown in Fig. 4, $[H^+]$ is fixed at 1.90 M and only $[BrO_3^-]$ is varied. For a small value of

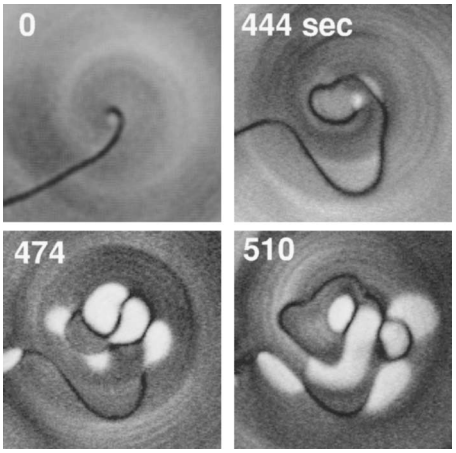

FIG. 13. Destabilization of a line defect and emergence of patches having a longer period following an increase of $[BrO_3^-]$ (from 0.120 to 0.124 M) at $t=0$. Images show the scalar field ΔV in a gray scale. The black lines are the line defects of P-2a spiral wave. The bulk gray area is $2\tau_a$ periodic whereas the white patched domains is $2\tau_b=3\tau_a$ periodic. The viewing area is 6×6 mm^2.

$[BrO_3^-]$, the system chooses a state of regular P-2 oscillatory spiral waves as shown in the gray-scale image of ΔV of Fig. 13 ($t=0$). $[BrO_3^-]$ is increased to 0.124 M, however, the underlying line defect becomes unstable, proliferate, and irregular ($t=444$ sec). Almost simultaneously, small patches of bright domains appear first around the core ($t=474$ sec) and begin to spread out ($t=510$ sec). For the (gray) value of ΔV reflecting the periodicity of local dynamics, we can state that the fragmented white domains have a distinct temporal dynamics that is different from the original P-2 dynamics of the bulk background, as well as from the P-1 dynamics of black line defects. In other words, a mixed state comprised of three distinct domains having different temporal dynamics has emerged. A much larger domain showing a MMP state with several unusual spiral waves is shown in Fig. 14(b). This new state distinguishes itself quite clearly from the initial P-2 spiral wave state of Fig. 14(a).

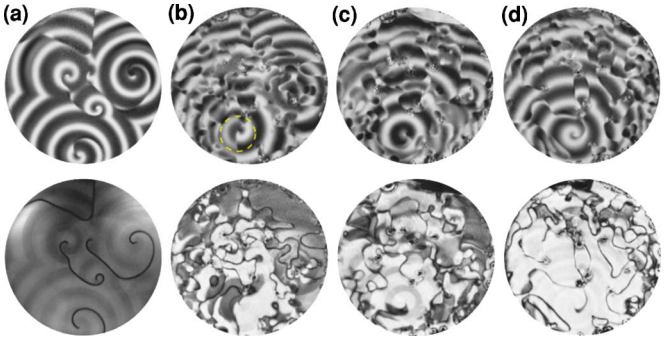

FIG. 14. (Color online) The transition of a P-2a state to a P-2b state via mixed-mode periodic wave state: (a) P-2a spiral waves ($[BrO_3^-]=0.116$ M, $\tau_a=18$ sec); (b) and (c) MMP spiral wave states ($[BrO_3^-]=0.128$ and 0.132 M, respectively, $\tau_b=27$ sec and $\tau_a=18$ sec) and (d) P-2b spiral waves ($[BrO_3^-]=0.135$ M, $\tau_b=24$ sec). Snapshot raw images are in the top row and the corresponding processed images showing scalar field ΔV are in the bottom row. The diameter of viewing area is 18 mm.

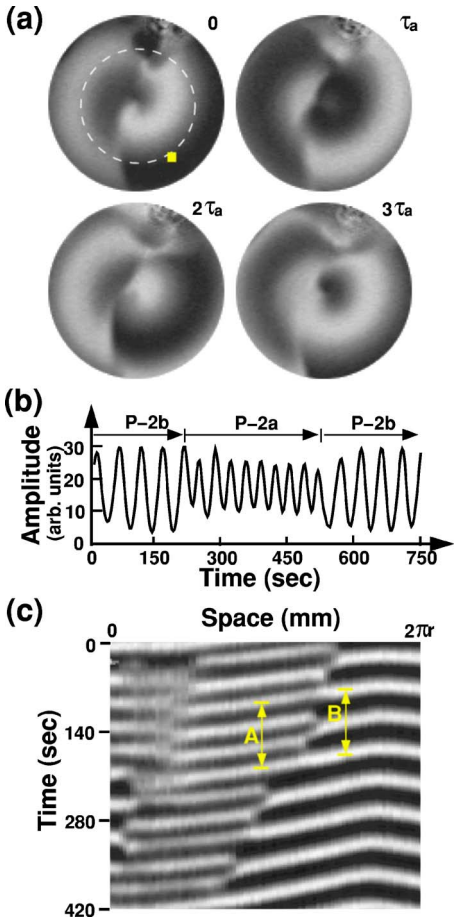

FIG. 15. (Color online) Structure and temporal evolution of a MMP spiral core in the encircled area of Fig. 14(b): (a) Snapshots of a MMP spiral taken at every $\tau_a=18$ sec 18 sec. The domain is divided by each different oscillating periods in left and right half of spiral core. Here τ_a is a fundamental period of P-1 oscillation in the domain of left side with a short oscillation. The diameter of viewing area is 3.2mm. (b) Local time series taken at the location of rectangular point in (a). The short (P-2a) and long periodic (P-2b) modes are mixed in time space. (c) Space-time plot taken along a circle centered at the spiral core with a radius $r=2.3$ mm.

One of the MMP spiral waves is analyzed in detail in Fig. 15. First of all, a sequence of snapshot images taken at an interval of $t=\tau_a$ is shown in Fig. 15(a). Here, $2\tau_a$ is the value of the P-2 spiral wave before the MMP transition. Notice that the gray-scale image does not repeat as a whole at the interval of $2\tau_a$. In other words, the system has acquired a different periodicity other than $2\tau_a$. This observation is clearer in the local time series of Fig. 15(b) that contains a new characteristic period $\tau_b=1.5\times\tau_a$. The existence of two different periodicities and their relationship are well captured in the space-time plot of Fig. 15(c). At the moving boundary separating the two different domains, $3\tau_a$ (marked by **A**) matches with $2\tau_b$ (marked by **B**). In other words, the oscillating domains are 2:3 mode-locked.

As $[BrO_3^-]$ is increased, the domain of P-2b spiral waves gradually replaces the initial state filled with P-2a spiral waves. This crossover is continuous as illustrated in the

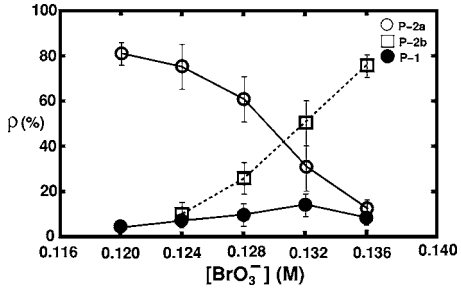

FIG. 16. Mean domain occupancy (ρ) vs $[BrO_3^-]$. The error bars reflect the spatiotemporal fluctuations over about 1 h.

sequence of images in Fig. 14 and quantified in Fig. 16 that depicts the proportion of each periodic domain.

B. Mixed state of P-2b spiral waves and chaotic domains

With a higher value of $[BrO_3^-]$, the state of P-2b spiral waves changes again by the emergence of some chaotic domains. A new mixed state containing two different domains form: one domain contains P-2b spiral waves and the other domain is highly turbulent. The turbulent domain contains a complex tangle of line defects that evolve very rapidly in space and time. Consequently, the local dynamics within the turbulent domain is quite irregular as Fig. 17(b) illustrates. This new mixed state is qualitatively very similar to the one formed by the aftermath of transverse instability of line defects of P-2 spiral waves discussed in Fig. 12. Within the turbulent domain, line defects proliferate irregularly to break up into many pieces, then grow again and annihilate in an unpredictable way.

Figure 18 highlights the boxed square area of Fig. 17(a) that more or less lies at the very volatile interface separating two qualitatively different domains. A picture taken at one instance is a regular state with P-2b spiral waves [see Fig. 18(a)]. At a different instance, however, the same view field represents a turbulent state having no discernible structure except for the existence of complex network of line defects [Fig. 18(b)]. In fact, these two different states alternate in time with no obvious pattern. The complex time course is visualized by quantifying the density ρ of underlying line defects. During the regular P-2b spiral wave state, ρ is quite low [as marked by **a** in Fig. 18(c)]. On the other hand, for the durations of the turbulent state ρ is rather high. More importantly, one notices that the turbulent activity involves high frequency fluctuations.

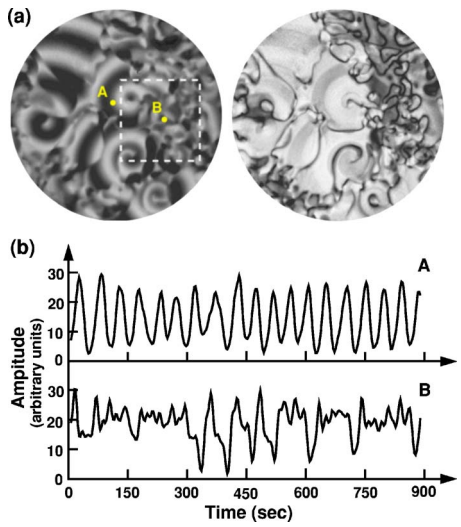

FIG. 17. (Color online) A coexisting pattern with a regular and chaotic domain (a) and two time series obtained each different periodic states, "**A**" and "**B**" (a). The diameter of viewing area is 18 mm and $[BrO_3^-]=0.140$ M.

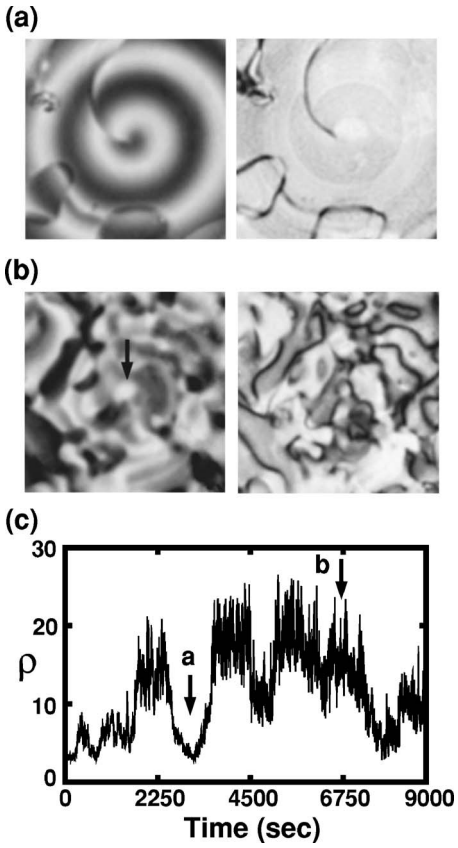

FIG. 18. Oscillating behavior of the regular and chaotic state revealed in the boxed area of Fig. 17(a): (a) Rgular P-2 spiral state with a spiraling line defect obtained at $t=2340$ sec. Some isolated bubble-shaped line defects exist around the core. (b) Spatiotemporal chaos with a tangle of line defects transformed from the regular P-2 state in (a), at $t=6750$ sec. The marked arrow indicates the spiral core. (c) density fluctuation of line defects for about 3 h. The density of line defects in regular P-2 spiral state (a) and chaotic state (b) is each obtained at the locations where the arrows "a" and "b" indicate. The density of line defect is calculated by binarizing (threshold at the low 20% of the total dynamic range) the scalar field ΔV. The viewing area is 8×8 mm^2 and $[BrO_3^-]=0.140$ M.

The chaotic domain grows at the expense of the regular P-2b domain upon a further increase of $[BrO_3^-]$ and the whole domain becomes chaotic around $[BrO_3^-]$ as shown in Fig. 19. Small wave segments with irregular shapes constantly appear and decay without any discernible pattern. Again, the complexity of the pattern is better understood by examining the image of ΔV [see Fig. 19(b)]. This particular turbulent state is visually quite similar to the one that had

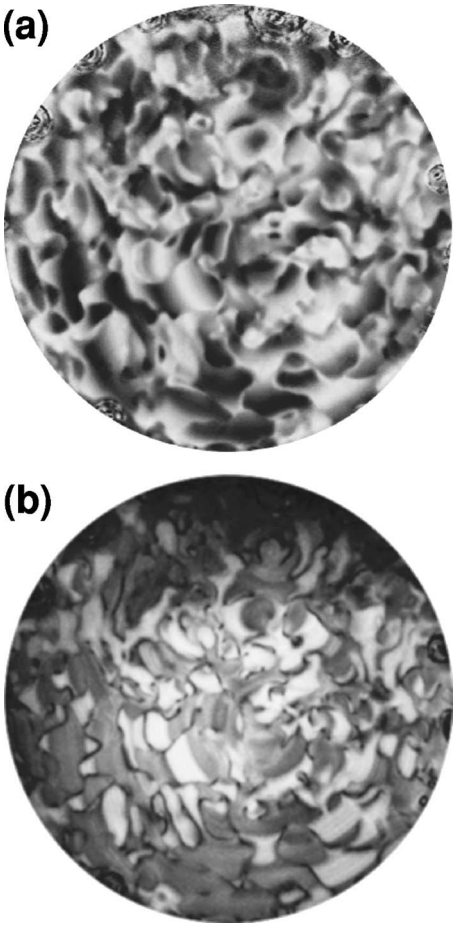

FIG. 19. Snapshot image of a turbulent state mediated by the line defects (a); and processed image revealing line defects and fragmented small domains of two periodic states (b). The diameter of the viewing area is 18 mm and $[BrO_3^-]=0.148$ M.

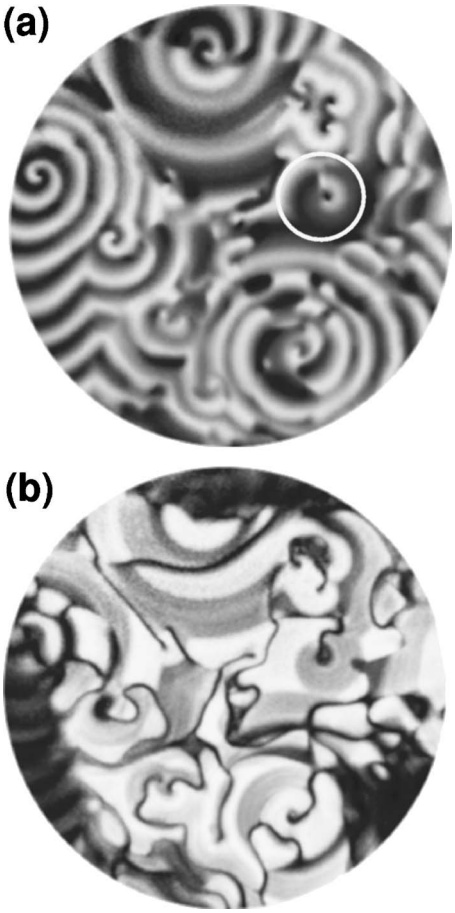

FIG. 20. Period-3 oscillatory spiral waves: (a) snapshot raw image; (b) processed snapshot image of ΔV. The diameter of viewing area is 18 mm and $[BrO_3^-]=0.050$ M.

arisen in the aftermath of a transverse instability of line defects in Fig. 12(c). Nevertheless, there is a significant difference: the complex wave state shown in Fig. 19 are comprised of three (the white, gray, and line defects) distinct fragmented domains, each having a different periodicity, while that of Fig. 12(c) has only two distinct domains (the gray and line defects). With the evolving mixture of two different periodic domains in conjunction with the compulsive evolution of the line defects, a long-time local time series at a fixed location is very irregular. Here, as well, the complexity of the local dynamics is not driven by the homogeneous kinetics but by the spatiotemporal dynamics of evolving periodic domains.

In this section we have investigated complex waves that arise along route **C** in the phase diagram of Fig. 4. Two interesting transitions are reported. First, we have found that a regular P-2 spiral wave state (P-2a) becomes a mixed-mode (2:3 mode-locked) periodic MMP spiral wave state that subsequently changes to a new P-2 spiral wave state (P-2b) having a 1.5 times longer period. Second, the P-2b spiral wave state becomes a spatio temporally turbulent state via an intermediate state with two competing domains of P-2b spiral waves and turbulent patches.

VII. PERIOD-3 OSCILLATORY SPIRAL WAVES

In a very small regime between P-2a and BR state of the phase diagram Fig. 4, spiral waves having a P-3 dynamics were observed (see Fig. 20)—i.e., rotating spiral waves produce a well defined P-3 local oscillation with a period of approximately 3τ, where τ is the fundamental period of the concerned system. Figure 21 focuses at the temporal evolution of a single P-3 oscillatory spiral wave. The whole spatial structure repeats at every 3τ. Three different peaks that comprise the time series of P-3 oscillation are marked by the symbols, **1**, **2**, and **3**, as depicted in Fig. 21(b). The amplitude of the peak marked by **2** is zero or almost negligible, while the amplitude of the primary peak **1** and that of the third peak **3** are quite close to each other. In the same light of explanation elucidating the emergence of P-2a spiral waves, one may view that the P-3 signal of Fig. 21(b) arises through a sequence of phase slips taking place at every 3τ, in other words, missing at every peak marked by **2**.

As the space-time plot of Fig. 21(c) clearly reveals, the P-3 spiral of Fig. 21 has a dynamic line defect (white dotted line) joining three different pairs of peaks. This line defect moves very slowly in the clockwise direction as the space-time plot well depicts. In principle, line defects of P-3 spiral state can take one of three different forms (type I connecting

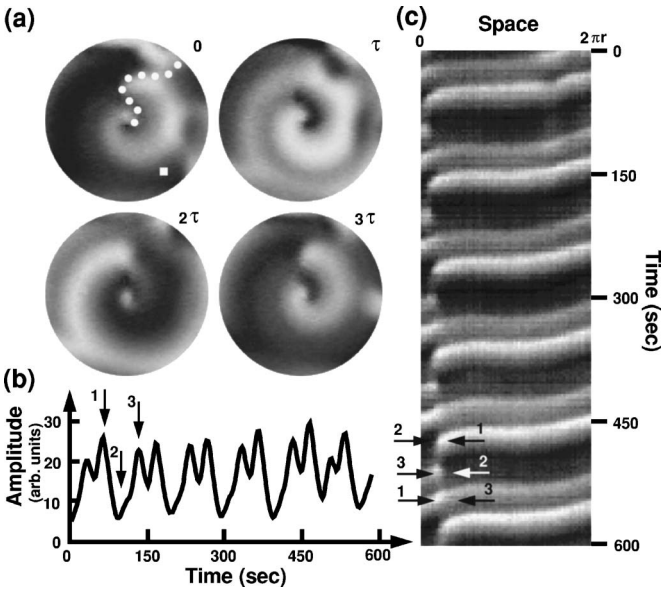

FIG. 21. Structure and temporal evolution of a P-3 spiral wave [encircled area in Fig. 20(a)]: (a) sequential snapshot images (taken at every $\tau=27$ sec) of a P-3 spiral wave having a single line defect—(overlaid) white dotted line. The radius of the viewing area is $r=3.2$ mm; (b) local time series taken at the square mark in (a); and (c) space-time plot taken along a circle centered at the spiral core with a radius $r=2.3$ mm. The arrows and numbers in (b) and (c) mark the position of three local peaks of P-3 oscillation.

2 and **1**, type II connecting **3** and **2**, and type III connecting **1** and **3**), while those for P-2 oscillatory spiral waves are simply connecting the up to the bottom state. From this viewpoint, the single line defect underlying the P-3 spiral wave is rather unusual for it alternates sequentially among three different types as the system evolves in time. As a consequence, the local dynamics right on the line defect is not P-1 but P-3 as three different types of loop exchange (see the schematic diagram of Fig. 22) take place there. This observation is in a good contrast to the earlier computational study by Goryachev *et al.*: they demonstrated the existence of P-3 spiral waves using a "super excitable" model system [38,39]. Interestingly, P-3 spiral wave states had two separate line defects spiraling out from the core.

The snapshot image of ΔV for the P-3 spiral state [see Fig. 20(b)] therefore contains line defects that vary from one place to the other in their thicknesses (or gray value). This is quite natural for there is no reason for spatially distributed line defects to be synchronized to each other. As the nature of P-3 line defects vary in time and as their shapes are highly irregular, the overall morphology of a P-3 spiral wave state is quite complex as Fig. 20(a) well illustrates. The processed image of ΔV for the P-3 state is much more complex than that of a typical P-2 state for the reason that the bulk area is also patched by three different types of domain, each having a different gray tone: the white, the gray, and the black banded areas, respectively.

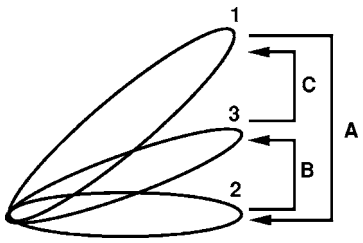

FIG. 22. Schematic diagram illustrating three different phase slips on a P-3 attractor.

VIII. CONCLUSIONS

This paper provides a comprehensive review on a number of different phenomena regarding complex-oscillatory spiral waves and their underlying line defects observed in a BZ experimental system. All together, eight different types of complex wave states are categorized in the phase space spanned by two key variables, $[H^+]$ and $[BrO_3^-]$. Their properties are discussed in detail. We have reported several different transitions that arise along three different passages on the two-dimensional phase space. A typical P-1 to P-2 spiral wave transition is discussed and a subsequent shape transition of a line defect followed by a meandering transition is elucidated following passage **A**. Two different types of turbulent transitions are observed, one along passage **B** and the other along passage **C**. The final time asymptotic turbulent states in both cases are characterized by fast proliferation and erratic annihilation of line defects. They can have a different origin: one was obtained through a transverse instability of line defects in a purely P-2 oscillatory state and the other was created through multiple steps of mixed-mode oscillations.

Many features of complex-oscillatory BZ spiral waves that we discussed here can be reproduced in several different systems. Most important of all, the existence of line defects in P-2 oscillatory media seems to be generic. Using a different BZ reaction-diffusion system employing a porous Vycor glass, Guo *et al.* have also found P-2 oscillatory spiral waves [82]. Very recently, our group was also able to produce P-2 oscillatory spiral waves in a cultured layer of cardiac cells (yet to be published). Furthermore, there are at least two different model systems (diffusively coupled Rössler oscillators and its hybrid Willamowski-Rössler oscillators) that exhibit complex periodic waves.

In the model systems, the line defects associated with P-2 spiral waves have been always found to be static in their time-asymptotic steady states: line defects move only for some transient periods following a change in the parameter values. On the contrary, the line defects so far observed in our BZ experimental system are always found to be dynamic except only for the special static case when it has the exact same form of a P-1 spiral wave. We believe that this difference originates from the fact that the spiral core in the Rössler system (and its hybrid Willamowski-Rössler system) is a *sink* for the inwardly moving phase waves generated from the system boundary, while it is a *source* in our experimental BZ system. In any cases, however, the dynamical properties of a line defect seems to have a close connection with its shape, in particular, its curvature. At least in the model systems curved line defects always evolve to a straight line defect extending between a spiral core and a pinning site along the system boundary.

We should also note that the BZ reaction has a more complex nature than that of the Rössler kinetics. It is well known that the BZ reaction in a continuously fed stirred reactor can exhibit a variety of different mixed-mode oscillations, and this particular property seems to support the observed mixed-mode periodic (MMP) wave states. In addition, one should realize that our experimental system is actually a quasi-two-dimensional system with strong concentration gradients across the gel thickness while the model systems are an ideal two-dimensional one. Therefore we cannot exclude the possibility of three-dimensional effects in our experiments, although all structures so far identified are at best quasi-two-dimensional—here, the term "quasi-two-dimensional" refers to the case that there is no hidden structure along the thin gel slab.

In our paper, the wave patterns that arise within the gel slab is basically considered as a quasi-two-dimensional one. A typical width of line defect—which is the smallest lateral object in our two-dimensional "projection image" is a few tenths of a millimeter being somewhat smaller but comparable to the total thickness of the gel where patterns form. It is also quite likely that waves form only within a narrower slab, which is much thinner than the total gel medium: in other words, there are chemical gradients across the gel slab, and only a small portion along its thickness may meet the right kinetic condition for the wave patterns. Such a case is well known in the studies of Turing patterns, for example, in Refs. [46,47]. In any case, we do not exclude the possibility that under some conditions nontrivial three-dimensional objects may arise in our system. We have not explored this possibility in any significant way. However, knowing that very analogous spiral waves and dynamics arise in several purely two-dimensional model reaction-diffusion systems [34–39,44] and in effectively two-dimensional self-oscillating monolayer tissues of cardiac cells strongly suggest us to interpret our experimental observations along the line of two-dimensional dynamics.

Various important issues are still unexplored. First, so far we have used only $[H^+]$ and $[BrO_3^-]$ as a control parameter. In other words, there are many other unexplored parameters. For example, the spiral wave dynamics depends sensitively on the change of the gel thickness or the residence time of chemical reagents in the reservoirs. Many more experiments are to be conducted to explore the huge untouched phase space. Second, we need to establish a theoretical framework for elucidating the dynamics of line defects in general. Although the existence of line defects is quite generic for P-2 oscillatory spiral waves in general, their spatiotemporal dynamics is not well understood. Among others, we need to derive a suitable equation of motion governing their dynamics. Along this line of viewpoint, we point out that Zhan and Kapral recently came up with an analytic solution of line defect based on the Archimedean splay state model [83] and Sandstede and Scheel is investigating full theoretical description of the line defect structure based on rigorous bifurcation analysis [84]. Third, all the phenomena regarding line defects in two-dimensional space can be generalized to three-dimensional space. Just as the studies on two-dimensional spiral waves in excitable media have been naturally extended to various issues of three-dimensional scroll waves, it is puzzling to see what would become the extension of one-dimensional line defect in three-dimensional space. A closely related issue is to carefully distinguish some possible artifacts created by two-dimensional projections of three-dimensional objects. Some earlier studies in fact suggest that even in a thin layer of BZ solution nontrivial wave structures can emerge [85–87]. Finally, we need to examine many other complex oscillatory systems to see which properties of line defects are generic and which are not.

ACKNOWLEDGMENT

This work was supported by Creative Research Initiatives of the Korea Ministry of Science and Technology.

[1] A. N. Zaikin and A. M. Zhabotinsky, Nature (London) **255**, 535 (1970).
[2] A. T. Winfree, Science **175**, 634 (1972).
[3] *Chemical Waves and Patterns*, edited by R. Kapral and K. Showalter (Kluwer, Dordrecht, 1995).
[4] Y. Kuramoto, *Chemical Oscillations, Waves, and Turbulence* (Springer-Verlag, Berlin, 1984).
[5] A. T. Winfree, *When Time Breaks Down* (Princeton University Press, Princeton, NJ, 1987).
[6] *Waves and Patterns in Chemical and Biological Media*, edited by H. L. Swinney and V. I. Krinsky (North-Holland, Amsterdam, 1992).
[7] O. Steinbock, V. Zykov, and S. C. Müller, Nature (London) **366**, 322 (1993).
[8] N. Manz, C. T. Hamik, and O. Steinbock, Phys. Rev. Lett. **92**, 248301 (2004).
[9] K. J. Lee and H. L. Swinney, Phys. Rev. E **51**, 1899 (1995).
[10] G. Etrl, Science **254**, 5039 (1991).
[11] V. K. Vanag and I. R. Epstein, Science **294**, 835 (2001).
[12] K. J. Lee, E. C. Cox, and R. E. Goldstein, Phys. Rev. Lett. **76**, 1174 (1996).
[13] E. Pálsson, K. J. Lee, R. E. Goldstein, J. Franke, R. H. Kessin, and E. C. Cox, Proc. Natl. Acad. Sci. U.S.A. **94**, 13719 (1997).
[14] F. Siegert and C. Weijer, Curr. Biol. **5**, 937 (1995).
[15] B. Vasiev, F. Siegert, and C. Weijer, Phys. Rev. Lett. **78**, 2489 (1997).
[16] S. Sawai, P. A. Thomason, and E. D. Cox, Nature (London) **433**, 323 (2005).
[17] J. Lechleiter, S. Girard, E. Peralta, and D. Clapham, Science **252**, 123 (1991).
[18] A. T. Winfree, Ann. N.Y. Acad. Sci. **591**, 190 (1990).
[19] A. T. Winfree, Science **266**, 1003 (1994).
[20] L. Glass, Phys. Today **49**(8), 40 (1996).
[21] R. A. Gray, A. M. Pertsov, and J. Jalife, Nature (London) **392**, 75 (1998).

[22] J. Jalife, Annu. Rev. Physiol. **62**, 25 (2000).
[23] J. N. Weiss, P.-S. Chen, T.-J. Wu, C. Siegerman, and A. Garfinkel, Ann. N.Y. Acad. Sci. **1015**, 122 (2004).
[24] A. Karma, Chaos **4**, 461 (1994).
[25] S. M. Hwang, K. H. Yea, and K. J. Lee, Phys. Rev. Lett. **92**, 198103 (2004).
[26] S. M. Hwang, T. Y. Kim, and K. J. Lee, Proc. Natl. Acad. Sci. U.S.A. **102**, 10363 (2005).
[27] E. A. Newman and K. R. Zahs, Science **275**, 844 (1997).
[28] M. E. Harris-White, S. A. Zanotti, S. A. Frautschy, and A. C. Charles, J. Neurophysiol. **79**, 1045 (1998).
[29] X.-Y. Huang *et al.*, J. Neurosci. **24**, 9897 (2004).
[30] K. S. Scott, *Chemical Chaos* (Clarendon Press, Oxford, 1991).
[31] M. C. Cross and P. C. Hohenberg, Rev. Mod. Phys. **65**, 851 (1993).
[32] K. J. Lee, Phys. Rev. Lett. **79**, 2907 (1997).
[33] J. Pearson, Science **261**, 189 (1993).
[34] A. Goryachev and R. Kapral, Phys. Rev. Lett. **76**, 1619 (1996).
[35] A. Goryachev and R. Kapral, Phys. Rev. E **54**, 5469 (1996).
[36] A. Goryachev, H. Chaté, and R. Kapral, Phys. Rev. Lett. **80**, 873 (1998).
[37] A. Goryachev, H. Chaté, and R. Kapral, Phys. Rev. Lett. **83**, 1878 (1999).
[38] A. Goryachev and R. Kapral, Int. J. Bifurcation Chaos Appl. Sci. Eng. **9**, 2243 (1999).
[39] A. Goryachev, H. Chaté, and R. Kapral, Int. J. Bifurcation Chaos Appl. Sci. Eng. **10**, 1537 (2000).
[40] M. Yoneyama, A. Fujii, and S. Maeda, J. Am. Chem. Soc. **117**, 8188 (1995).
[41] We speculate that in their case the oxygen gradient along the z axis may have provided a continuous variation of oxygen concentration that causes a period-doubling (or wavelength-doubling) bifurcation at some point along the z axis. As a consequence, there forms a regular spiral at the bottom while a wavelength-doubled spiral forms at the top.
[42] J.-S. Park and K. J. Lee, Phys. Rev. Lett. **83**, 5393 (1999).
[43] J.-S. Park and K. J. Lee, Phys. Rev. Lett. **88**, 224501 (2002).
[44] J.-S. Park, S.-J. Woo, and K. J. Lee, Phys. Rev. Lett. **93**, 098302 (2004).
[45] Q. Ouyang and H. L. Swinney, Nature (London) **352**, 610 (1991).
[46] K. J. Lee, W. D. McCormick, Z. Noszticzius, and H. L. Swinney, J. Chem. Phys. **96**, 4048 (1992).
[47] V. Castets, E. Dulos, J. Boissonade, and P. De Kepper, Phys. Rev. Lett. **64**, 2953 (1990).
[48] S.-J. Woo, J. Lee, and K. J. Lee, Phys. Rev. E **68**, 016208 (2003).
[49] Q, Ouyang and J. M. Flesselles, Nature (London) **379**, 143 (1996).
[50] L. Q. Zhou and Q. Ouyang, Phys. Rev. Lett. **85**, 1650 (2000).
[51] Q. Ouyang, H. L. Swinney, and G. Li, Phys. Rev. Lett. **84**, 1047 (2000).
[52] H. Guo, L. Li, and Q. Ouyang, J. Chem. Phys. **118**, 5038 (2003).
[53] A. L. Belmonte, Q. Ouyang, and J. M. Flesselles, J. Phys. II **7**, 1425 (1997).
[54] L. Q. Zhou and Q. Ouyang, J. Phys. Chem. A **105**, 112 (2001).
[55] S. Alonso, F. Saqués, and A. S. Mikhailov, Science **299**, 1722 (2003).
[56] R. A. Schmitz, K. R. Graziani, and J. L. Hudson, J. Chem. Phys. **67**, 3040 (1977).
[57] R. H. Simoyi, A. Wolf, and H. L. Swinney, Phys. Rev. Lett. **49**, 245 (1982).
[58] K. Showalter, R. M. Noyers, and K. Bar-Eli, J. Chem. Phys. **69**, 2514 (1978).
[59] J. Maselko and H. L. Swinney, J. Chem. Phys. **85**, 6430 (1986).
[60] P. Richetti, J. C. Roux, and A. Arneodo, J. Chem. Phys. **86**, 3339 (1987).
[61] K. Coffman *et al.*, J. Chem. Phys. **86**, 119 (1987).
[62] F. Argoul, A. Arneodo, P. Richetti, and J. C. Roux, J. Chem. Phys. **86**, 3325 (1987).
[63] P. Richetti, J. C. Roux, F. Argoul, and A. Arneodo, J. Chem. Phys. **86**, 3339 (1987).
[64] L. Györgyi and R. J. Field, J. Phys. Chem. **95**, 6594 (1991).
[65] M. Rachwalska and A. L. Kawczyński, J. Phys. Chem. A **103**, 3455 (1999).
[66] M. Rachwalska and A. L. Kawczyński, J. Phys. Chem. A **105**, 7885 (2001).
[67] A. T. Winfree, Science **181**, 937 (1973).
[68] D. Barkley, Phys. Rev. Lett. **72**, 164 (1994).
[69] L. Q. Zhou and Q. Ouyang, Phys. Rev. Lett. **85**, 1650 (2000).
[70] S. M. Hwang, W. G. Choe, and K. J. Lee, Phys. Rev. E **62**, 4799 (2000).
[71] G. Li, Q. Ouyang, V. Petrov, and H. L. Swinney, Phys. Rev. Lett. **77**, 2105 (1996).
[72] M. G. Rosenblum, A. S. Pikovsky, and J. Kurths, Phys. Rev. Lett. **76**, 1804 (1996).
[73] U. Parlitz, L. Junge, W. Lauterborn, and L. Kocarev, Phys. Rev. E **54**, 2115 (1996).
[74] K. J. Lee, Y. Kwak, and T. K. Lim, Phys. Rev. Lett. **81**, 321 (1998).
[75] The passage of the wave tip is traced only when the core wave profile is in "up state," since the position of the tip becomes ill-defined when the state of the core region goes to "down state."
[76] J. Davidsen, R. Erichsen, R. Kapral, and H. Chaté, Phys. Rev. Lett. **93**, 018305 (2004).
[77] J. Davidsen and R. Kapral, Phys. Rev. Lett. **91**, 058303 (2003).
[78] O. Decroly and A. Goldbeter, Proc. Natl. Acad. Sci. U.S.A. **79**, 6917 (1982).
[79] A. Arneodo, F. Argoul, J. Elezgaray, and O. Richetti, Physica D **62**, 134 (1993).
[80] M. T. Koper, P. Gaspard, and J. H. Sluyters, J. Phys. Chem. **97**, 8250 (1992).
[81] H. P. Meissner, Nature (London) **262**, 502 (1976).
[82] H. Guo, L. Li, H. Wang, and Q. Ouyang, Phys. Rev. E **69**, 056203 (2004).
[83] M. Zhan and R. Kapral, Phys. Rev. E **72**, 046221 (2005).
[84] B. Sandstede and A. Scheel, SIAM J. Appl. Dyn. Syst. **3**, 1 (2004).
[85] K. I. Agladze, V. I. Krinsky, A. V. PanFilov, H. Linde, and L. Kuhnert, Physica D **39**, 38 (1989).
[86] A. M. Zhabotinsky, S. C. Müller, and B. Hess, Physica D **49**, 47 (1991).
[87] S. Mironov, M. Vinson, S. Mulvey, and A. Pertsov, J. Phys. Chem. **100**, 1975 (1996).